RSC Advances

ROYAL SOCIETY OF CHEMISTRY

www.rsc.org/advances

Journal Name

ARTICLE

Facile synthesis of ultra-small ruthenium oxide nanoparticles anchored on reduced graphene oxide nanosheets for high-performance supercapacitors

Received 00th January 20xx,
Accepted 00th January 20xx

DOI: 10.1039/x0xx00000x

www.rsc.org/

F. Z. Amir,[a*] V. H. Pham,[b] J. H. Dickerson[b]

Herein, we report a facile, low cost, and environmentally friendly approach to prepare reduced graphene oxide–ruthenium oxide hybrid (RGO-RuO_2) materials for supercapacitor electrode applications by *in situ* sol-gel deposition of RuO_2 nanoparticles on the surface of graphene oxide (GO), followed by a reduction of GO in a strong alkaline medium at a low temperature. The combination of the sol-gel route and the reduction of graphene oxide at low temperature resulted in ultrafine, hydrated amorphous RuO_2 particles with the size of only 1.0 – 2.0 nm, which uniformly decorated the surfaces of RGO sheets. The obtained RGO-RuO_2 supercapacitor exhibited excellent electrochemical capacitive performance in a 1M H_2SO_4 electrolyte with a specific capacitance more than 500 F/g at a current density of 1.0 A/g and high rate performance with the capacitance retention of 86 % when increasing 20 times the current density, from 1.0 to 20.0 A/g in a two-electrode test cell configuration. The RGO-RuO_2 system also showed good cycling stability with a capacitance retention of 87 % after 2000 cycles. The excellent capacitive properties of RGO-RuO_2 could be attributed to the uniform anchoring of ultra-small, hydrated amorphous RuO_2 nanoparticles on the surface of RGO sheets, resulting in synergistic effects between them. The developed approach represents an exciting direction for enhancing the device performance of the graphene-metal oxides composites supercapacitors and can be used for designing the next generation of energy storage devices.

Introduction

Supercapacitors, a class of electrochemical energy storage devices with high power capacity, pulse power supply, exceptionally long cycling life, fast dynamics of charge propagation and low maintenance cost, are considered as one of the most important devices for the next generation of energy storage.[1-3] Bridging conventional capacitors and batteries, supercapacitors have several applications, such as energy back-up systems, portable devices, power tools, and hybrid electric vehicles.[1-4] Supercapacitors can be classified into two categories based on the charge-storage mechanism: electrical double-layer capacitors (EDLCs) and pseudocapacitors. EDLCs achieve energy storage by forming a double layer of electrolyte ions on the surface of the conductive electrodes. Hence, high specific surface area and electrical conductivity of the electrode are crucial to ensure good performance of EDLCs.[1,2] Carbon-based materials with high surface area, such as activated carbons, mesoporous carbons, carbon nanotubes, carbon aerogels, and recently graphene, are the most common materials in EDLCs. EDLCs composed of carbon electrodes have shown very high power density due to their fast kinetics on the adsorption or desorption of electrolyte ions; however, their relatively low energy density significantly limits their practical applications. In contrast to EDLCs, the capacitance of a pseudocapacitor comes from faradaic redox reactions at the electrode/electrolyte surface.[4] Transition metal oxides and conducting polymers such as RuO_2, MnO_2, V_2O_5, polyaniline, and polypyrrole, are among the most common pseudocapacitive materials. Although pseudocapacitive materials could possess a specific capacitance that is 10-100 times higher than that of EDLCs, they usually suffer from relatively low power density and instability during cycling.[5,6] The incorporation of pseudocapacitive materials into EDCL material matrices, creating hybrid structures, is the most common strategy to achieve both high power density and energy density as well as good cycling stability of supercapacitors.

Graphene, a one-atom-thick two dimensional (2D) single layer of sp^2–bonded carbon, is considered as an ideal EDLC electrode material due to its extremely large surface area, extraordinarily high electrical conductivity, good chemical stability, and high mechanical strength.[1-3] On the other hand, RuO_2 has been the most extensively studied candidate for pseudocapacitor electrode materials, given its wide potential window, highly reversible redox reaction, remarkably high specific capacitance, high rate capacity and long cycle life.[4, 6] Combining the ideal EDLC electrode material with the most promising pseudocapacitive material is expected to create the best electrode material for supercapacitors. So far, several

[a] Department of Chemistry, Physics and Geology, Winthrop University, Rock Hill, SC 29733,USA
[b] Center of Functional Nanomaterials, Brookhaven National Laboratory, Upton, NY 11973, USA

attempts have been made to combine these two kinds of materials.[7-17] However, the capacitive performance of RGO-RuO_2 nanocomposites has varied, ultimately depending on the dispersion morphology and crystallinity of RuO_2 particles on RGO. To obtain high capacitive performance, RuO_2 must be in the form of small sized, hydrated, amorphous nanoparticles, uniformly anchored on the surface of an RGO single sheet.[6] Since the pseudocapacitance of RuO_2 comes from the reversible faradaic redox reaction, the hydrated amorphous structure of RuO_2 nanoparticles allows the redox reactions to occur not only at the surface (like crystalline RuO_2 nanoparticles) but also within the inner parts of the RuO_2 nanoparticles. The smaller the size of the RuO_2 nanoparticles is, the higher the specific surface area is. Thus, more metal centers will be able to provide multiple redox reactions resulting in higher specific capacitance values .[6]

The uniform anchoring of RuO_2 nanoparticles onto the surface of RGO sheets provides conduction paths that enable electrons to be easily transferred from the current collector to RuO_2 nanoparticles and vice versa. So far, the synthesis of RGO-RuO_2 can be classified into two strategies based on the RGO precursor. The first and most common approach is using RGO as a precursor in sol-gel or hydrothermal processes.[7-10, 12] In this approach, RGO is first prepared by the chemical reduction or thermal exfoliation/reduction of GO and the resultant material's use as a precursor in a sol-gel or a hydrothermal process. However, since RGO is usually in an aggregated or a restacked form, which is not exfoliated or well dispersed in common polar solvents (e.g. water, methanol, ethanol or isopropanol), the deposition of RuO_2 nanoparticles on aggregated RGO sheets results in a loss of the effective surface area. More importantly, since RGO has fewer oxygen functional groups on the surface, which might act as nucleation and anchoring sites for the oxide formation, the density of RuO_2 nanoparticles anchored on the surface of RGO is less. Therefore, RuO_2 nanoparticles have the tendency to grow during the hydrothermal process, which is unfavorable for capacitive properties.[15] Surfactants, like polyvinylpyrrolidone, polyelectrolytes, or poly (diallyldimethylammonium chloride), have been used as a stabilizer to improve the dispersion of RGO in water and the dispersion of RuO_2 nanoparticles on RGO sheets.[12,16] However, these stabilizers, which are absorbed on the surface of RGO-RuO_2, are undesirable as a component of electrode materials and must be removed prior to the further use of RGO-RuO_2. A second approach involves GO as a precursor in hydrothermal processes. In contrast to RGO, GO is completely exfoliated and dispersed in polar solvents and has abundant oxygen functional groups on the surface, providing numerous sites for RuO_2 deposition. As a result, small and uniform RuO_2 nanoparticles can decorate the surface of GO sheets. However, since GO is an insulating material, the hydrothermal process is usually carried out to reduce GO, recovering the electrical conductivity.[14-16]Unfortunately, high temperature hydrothermal processes (180-200 ^{o}C) result in the recrystallization of RuO_2, which is undesirable.[15-16]

In this study, we have designed a facile approach to prepare RGO-RuO_2 hybrid composites through the *in-situ* sol-gel deposition of RuO_2 nanoparticles on the surface of GO, followed by a reduction of GO in a strong alkaline medium at low temperature. The combination of sol-gel techniques and the reduction of GO at low temperatures resulted in ultrafine, hydrated amorphous RuO_2 nanoparticles of a diameter 1.0 – 2.0 nm that uniformly decorated the surfaces of RGO sheets. The electrochemical capacitive properties of RGO-RuO_2 were characterized using a two-electrode test cell configuration in 1M H_2SO_4 and 1M Na_2SO_4 electrolyte solutions in the potential window of 1.0 and 1.5 V, respectively. The RGO-RuO_2 exhibited excellent electrochemical capacitive performance in H_2SO_4 with a specific capacitance more than 500 F/g at a current density of 1.0 A/g. This material also exhibited high rate performance with a capacitance retention of 86 % when increasing the current density by 20 times, from 1.0 to 20.0 A/g. RGO-RuO_2 also displayed good cycling stability with a capacitance retention of 87 % after 2000 cycles.

Experimental

Preparation of GO

GO was synthesized from expanded graphite by the modified Hummers method, described elsewhere.[20] Briefly, 200 mL of concentrated H_2SO_4 was charged into a 1000 mL beaker equipped with a mechanical stirrer (Teflon impeller). Two grams of expanded graphite was gradually added under stirring to make a suspension. Then, 15 g of $KMnO_4$ was slowly added. The temperature was then elevated to 35°C, and the suspension was stirred for 2 h. The beaker was then chilled in an ice bath, and 500 mL of deionized water was slowly added to maintain a temperature below 70°C. The mixture was stirred for 1 h and subsequently diluted with 3.0 L of deionized water. Twenty mL of H_2O_2 (30 wt %) was slowly added, and vigorous bubbles appeared as the color of the suspension changed from dark brown to yellow. The suspension was centrifuged and then washed with 1M HCl solution four times to remove manganese compound residues. Subsequently, the H_2SO_4 was removed by copiously centrifuging and washing with deionized water. The obtained GO existed as a highly viscous solution.

Preparation of RGO-RuO_2 hybrid

The as-prepared GO was diluted to a concentration of 0.5 mg/ml and sonicated for 10 min to obtain a homogenous solution. 622 mg of ruthenium chloride hydrate ($RuCl_3.xH_2O$, Ru content 40-49%) was then added into 200 mL of GO solution (0.5 mg/mL) under mixing. Then, the suspension was neutralized with 1M NaOH to a pH ~7 and stirred for 12 h at room temperature to obtain GO-RuO_2. Subsequently, the pH of the GO-RuO_2 suspension was adjusted by adding 1M NaOH to 12, and the suspension was aged at 90°C for 12 h to deoxygenation of GO.[21] The RGO-RuO_2 suspension was repeatedly centrifuged and washed with deionized water and freeze-dried. The resulting RGO-RuO_2 was denoted as the *as-prepared* RGO-RuO_2. Finally, as-prepared RGO-RuO_2 was

annealed at 150 °C for 2 h to obtain annealed RGO-RuO_2 (a-RGO-RuO_2). To provide a materials standard for characterization, RGO was prepared following the above procedure without the additional ruthenium chloride.

Characterization

The morphologies of the a-RGO-RuO_2 materials were characterized by scanning electron microscopy (SEM, JEOL 7600F) and transmission electron microscopy (TEM, JEOL 1400). The elemental mapping of a-RGO-RuO_2 was provided by energy dispersive X-Ray spectroscopy (EDS) and was performed on JEOL 7600F. Structural analysis was carried out on the Rigaku Ultima III x-ray diffractometer with CuK_α radiation (λ=0.15418nm) at 40 kV and 44 mA. Thermogravimetric analysis (TGA) was performed under argon and air atmospheres at a heating rate of 5 °C min^{-1} (Perkin Elmer).

Electrode preparation and electrochemical measurements

The a-RGO-RuO_2 electrodes were prepared by mixing a-RGO-RuO_2 with carbon black and polytetrafluoroethylene (PTFE) in a mass ratio of 80:15:5 in ethanol to make a slurry. The mixture was sonicated for 5.0 min. The slurry was partially dried to make a paste, which was subsequently casted and pressed onto stainless steel and nickel foam (1.5 x 1.5 cm^2) substrates that were used as current collectors. All casts were dried at 100 °C for 3 h. The mass of a-RGO-RuO_2 was about 4.5–5.0 mg/cm^2. Prior to the electrochemical measurement, the electrodes were soaked in each of the electrolytes for 12 h.

The capacitive performance of the a-RGO-RuO_2 was characterized for a two-electrode configuration. Two identical electrodes, separated by a filter paper separator in 1M Na_2SO_4 and 1M H_2SO_4 electrolytes, were sandwiched in a supercapacitor test cell (EQ-STC split flat cell, MTI Corp.) Cyclic voltammetry (CV) measurements were performed on a potentiostat/galvanostat PARSTAT 2273 (Princeton Applied Research), and galvanostatic charge–discharge (GCD) tests were conducted on an Arbin battery tester BT2000 (Arbin Instrument) in the potential range of 0 - 1.5 V and 0 - 1.0 V for 1M Na_2SO_4 and 1M H_2SO_4, respectively. Electrochemical impedance spectroscopy (EIS) tests were performed over a frequency range from 0.01 Hz to 100 kHz at an open circuit potential with an AC perturbation of 10.0 mV. The mass specific capacitance, energy density, and power density were calculated according to the following equations: [22, 23]

$$C_{sp} = 4\left(\frac{I\Delta t}{m\Delta V}\right) \quad (1)$$

$$E = \frac{1}{8}\,C(\Delta V)^2 \quad (2)$$

$$P = \frac{E}{\Delta t} \quad (3)$$

where C_{sp} is the specific capacitance, I is the constant discharge current, Δt is the discharging time, m is the mass of two electrode, ΔV is the voltage drop upon discharging, E is the energy density, and P is the power density.

Results and discussion

The synthesis of a-RGO-RuO_2 hybrids, as illustrated in Fig. 1, involved sol-gel techniques followed by the deoxygenation of GO. By adding the $RuCl_3.xH_2O$ into the GO solution, the viscosity of the solution significantly increased because of the strong interactions between cationic Ru^{3+} and the oxygen functional groups (hydroxyl, epoxy and carboxyl groups) on the surface and the edge of the GO sheets. This led to abundant cross-linking between the GO sheets.[24] The abundant oxygen functional groups of GO strongly interact with Ru^{3+}, making them the active sites for nucleation and anchoring of the RuO_2 nanoparticles during the sol-gel process. This results in uniform coating of RuO_2 nanoparticles on the surface of GO sheets. Although the GO was slightly reduced during the sol-gel process,[15] that reduction is insufficient to recover the electrical conductivity that is vital for effective capacitive electrode materials. The further reduction of GO was carried out in a strong alkaline medium at low temperature to prevent the growth and recrystallization of RuO_2 nanoparticles. The reduction of GO in an alkaline medium is well-known as an effective and green approach to prepare RGO. More interestingly, unlike other reduction methods, the reduction of

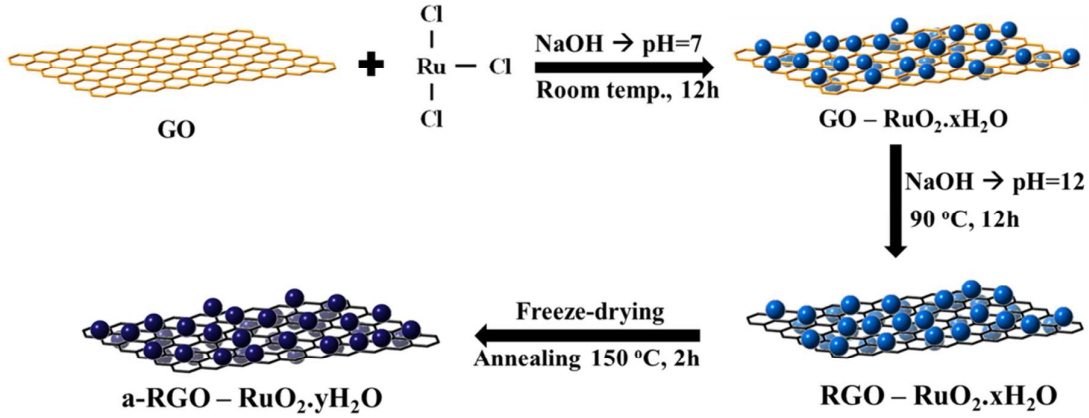

Figure 1. Schematic illustration of the preparation procedure for the a-RGO-RuO_2 hybrid.

GO in an alkaline medium yields in highly dispersible RGO.[21]

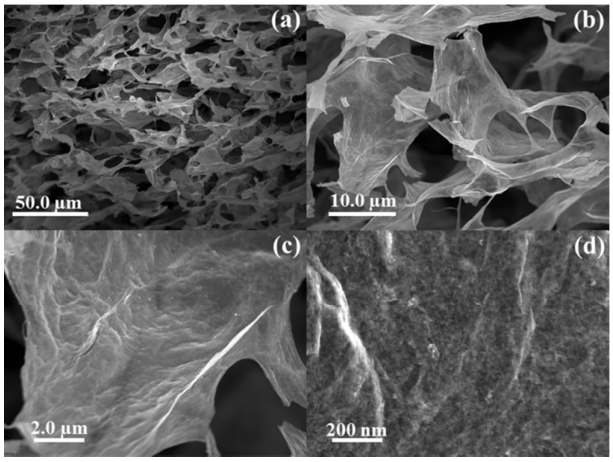

Figure 2. (a-d) SEM images of a-RGO-RuO_2 at different magnifications.

After the alkaline reduction, the coagulated RGO-RuO_2 particles were observed to be re-dispersible in water or ethanol by mild sonication. Annealing the as-prepared RGO-RuO_2 at 150 ^oC for 2 hours optimally removed both absorbed and chemically bound water from the RuO_2 nanoparticles to improve the capacitive performance of RGO-RuO_2.[6, 7, 8-10, 25, 26] Higher annealing temperatures may result in complete dehydration and recrystallization of RuO_2 nanoparticles, leading to a capacitance decrease.

Fig. 2 (a-d) shows SEM images of a-RGO-RuO_2, revealing a three-dimensional porous structure consisting of interconnected flakes with pore sizes as large as ten microns. The RuO_2 nanoparticles were densely and homogeneously anchored across the wrinkled RGO sheets. To confirm the uniform dispersion of the RuO_2 nanoparticles on RGO sheets, EDS mapping was performed, as shown in Fig. 3 (b-d). Three elements, carbon (C), oxygen (O) and ruthenium (Ru), were observed in the map; the densities and the distribution of C, Ru and O matched the topology of the corresponding a-RGO-RuO_2.This suggested a uniform distribution of RuO_2 nanoparticles on RGO sheets. The elemental compositions of a-RGO-RuO_2, as determined by EDS, were 46.18, 27.85 and 25.97 wt% for C, O and Ru, respectively.

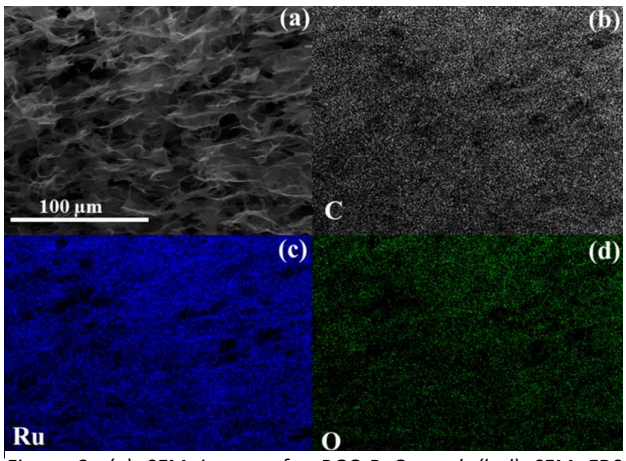

Figure 3. (a) SEM image of a-RGO-RuO_2 and (b-d) SEM EDS mapping of (a).

The microstructure of a-RGO-RuO_2 was further characterized by TEM. The low magnification of TEM micrographs in Fig. 4(a) showed the micron-sized wrinkled RGO sheets, which were densely coated by RuO_2 nanoparticles. Although the suspension was sonicated for 1 minute during the TEM sample preparation, no unbound RuO_2 nanoparticles were found, indicating strong interactions between RuO_2 nanoparticles and RGO sheets. The high magnification TEM image in Fig. 4b revealed ultra-small RuO_2 nanoparticles with the size of only 1.0-2.0 nm, disorderedly anchored on the surface of the RGO sheet, creating nanopores and nanochannels which may act as electrolyte reservoirs, facilitating the ions transportation during electrochemical redox reactions. The inset of Fig. 4c displays a TEM diffraction pattern of a-RGO-RuO_2 consisting of diffuse ring diffraction patterns with no discrete reflections; this indicated that a-RGO-RuO_2 has an amorphous structure.

Figure 5 shows the x-ray diffraction (XRD) patterns of GO, RGO, as-prepared RGO-RuO_2 and a-RGO-RuO_2. The XRD pattern of GO showed a strong peak at 10.6^o, corresponding to the (002) reflection with interlayer spacing of 8.32 Å. After the alkaline reduction, a broad peak was observed at 23^o, corresponding to an inter-sheet spacing of 3.8 Å, which is distinctly smaller than the interspacing between GO sheets due to the removal of the oxygen functional groups on the surface of RGO.[27] The XRD patterns of the as-prepared RGO-

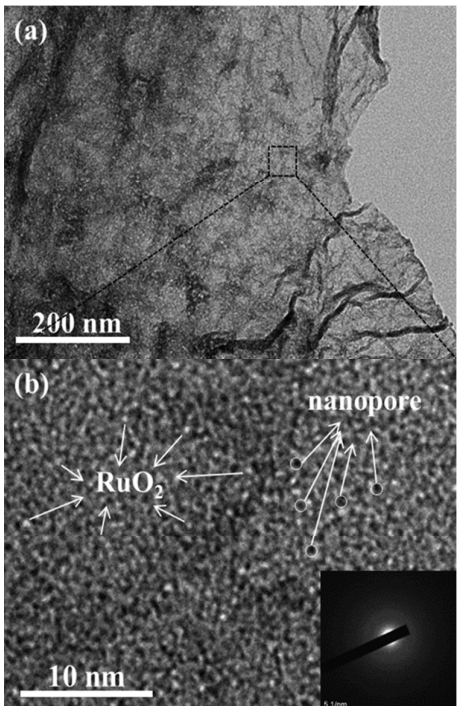

Figure 4. (a&b) TEM images and the inset show TEM diffraction of a-RGO-RuO_2

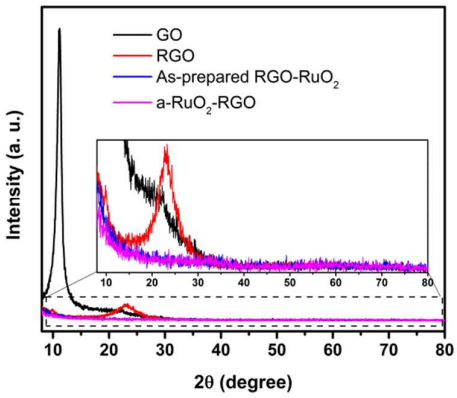

Figure 5. XRD patterns of GO, RGO, as-prepared RGO-RuO_2 and a-RGO-RuO_2

RuO_2 and a-RGO-RuO_2 do not exhibit peaks between 10 to 80°, implying that both the as-prepared RGO-RuO_2 and the a-RGO-RuO_2 are amorphous. Moreover, the disappearance of the broad RGO peak at 23° indicates that the anchored RuO_2 nanoparticles on the surface of RGO sheets act as a spacer, effectively preventing the restacking of RGO sheets.

The thermal stability of a-RGO-RuO_2 in air and in an inert atmosphere was characterized by TGA as shown in Fig. 6. The TGA curve of a-RGO-RuO_2 in argon atmosphere shows appropriately 8.7 and 14.6 % mass losses at 150 and 600 °C, respectively. The first mass loss can be attributed to the evaporation of the absorbed water, whereas the second mass loss is ascribed to the removal of chemically bound water in hydrated RuO_2 and the removal of labile oxygen functional groups of RGO, such as hydroxyl, epoxy and carbonyl groups.[7,14, 20, 25] The significant mass loss of a-RGO-RuO_2 at temperatures lower than 150 °C indicated that RuO_2 exists in a hydrous form after thermal annealing, which is essential for enhancing the diffusion of cations inside the electrode material.[6] The TGA of a-RGO-RuO_2 in air showed almost an identical mass loss to that of a-RGO-RuO_2 in an inert atmosphere at temperatures lower than 150 °C. However, the significant mass loss was observed in the temperature range of 150 - 350 °C, which can be mainly attributed to the oxidation of RGO under the catalytic influence of RuO_2 nanoparticles.[28] The residue of a-RGO-RuO_2 was almost unchanged, approximately 72.6 wt%, at temperature higher than 400 °C, which can be assigned to the mass of RuO_2. The RGO content

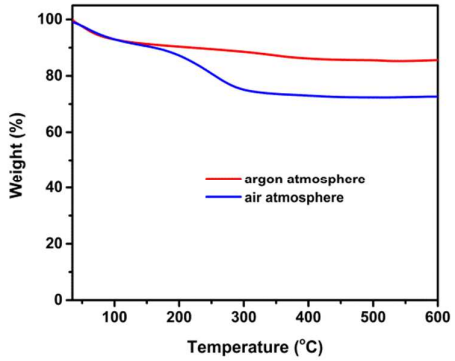

Figure 6. TGA of a-RGO-RuO_2 in argon and air atmospheres

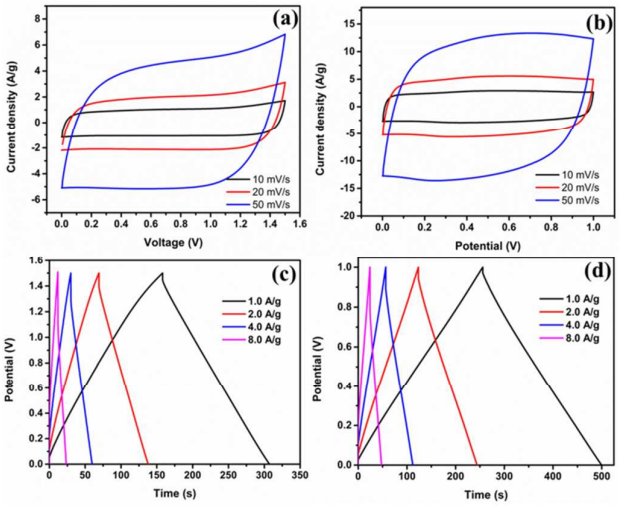

Figure 7. (a, b) CV and (c, d) charge-discharge curves of a-RGO-RuO_2 in Na_2SO_4 and H_2SO_4 electrolytes, respectively.

in a-RGO-RuO_2 could be estimated to be in a range of 12.9 – 18.8 wt%. The first value (12.9 wt%) was estimated from the difference of the residues of a-RGO-RuO_2 at 600 °C in argon and air atmospheres whereas the second value (18.8 wt%) came from the difference in the residues of a-RGO-RuO_2 at 150 °C and 600 °C in air atmosphere. Correspondingly, the mass ratio of RGO:RuO_2 was about 1:3.8 to 1:5.6, which is closed to the theoretical input value of GO:RuO_2 (1:4.0).

The electrochemical capacitive behavior of a-RGO-RuO_2 was evaluated by CV and GCD techniques. Fig. 7(a&b) shows CV curves of a-RGO-RuO_2 at different scan rates in 1M Na_2SO_4 (neutral) and 1M H_4SO_4 (acidic) electrolytes, respectively. Taking advantage of the neutral electrolyte, the capacitive properties of a-RGO-RuO_2 in Na_2SO_4 were characterized in the potential window of 0.0-1.5 V to improve the energy density.[17,29] The CV curves of a-RGO-RuO_2 in both electrolytes were nearly rectangular, and no redox peak was observed, indicating that the a-RGO-RuO_2 had nearly ideal capacitive behavior. The absence of the redox peak can be explained by the very fast reversible redox reaction that occurred on the surface of RuO_2 nanoparticles, which can be attributed to the ultra-small size of the hydrous RuO_2 nanoparticles. According to Zhang *et al.*,[6] the redox reaction can occur at a depth of 2 nm from the surface of the particle; considering the ultra-small size of the RuO_2 nanoparticles, the redox reaction occurred on their surface. The current density values of the CV curves of a-RGO-RuO_2 in H_2SO_4 were more than twice that of a-RGO-RuO_2 in Na_2SO_4 at the same scan rate, indicating that the a-RGO-RuO_2 has higher specific capacitance in H_2SO_4. The GDC curves of a-RGO-RuO_2 in Fig. 7(c&d) were symmetrically triangular, which is another indication of ideal capacitive behavior. A small IR drop was observed at the beginning of the discharge curve, especially for a-RGO-RuO_2 in H_2SO_4, implying the low internal resistance within the electrode.

The specific capacitances of a-RGO-RuO_2 calculated from the discharge curves were shown in Fig. 8(a). The specific capacitances of a-RGO-RuO_2 in H_2SO_4 were 509.4 and 439.2 F/g at current densities of 1.0 and 20.0 A/g, respectively. These

Table 1. Summary of specific capacitances of RGO-RuO_2 collected from the literature.

Material	Synthesis method	Structure	RuO_2 content	Testing configuration	Specific capacitance	Ref.
RuO_2-f-HEG	Sol-gel + annealing at 350 °C, 2 h	Crystalline	25 wt%	Two-electrode	265 F/g at scan rate 10 mV/s	8
RuO_2/GNs	Sol-gel + annealing at 150 °C, 6 h	Amorphous	36 wt%	Two-electrode	365 F/g at scan rate 5 mV/s	10
RGO-RuO_2	Sol-gel + annealing at 150 °C, 2 h	Not reported	86.9 wt%	Two-electrode	400 F/g at current density of 1.0 A/g	9
GRA-6	Hydrothermal + annealing at 150 °C, 6h	Partial crystalline	45 wt%	Three-electrode	471 F/g at current density of 0.5 A/g	11
ROGSC	Sol-gel + annealing at 150 °C, 2 h	Partial crystalline	50.4 wt%	Three-electrode	570 F/g at scan rate of 1 mV/s	7
RuO_2/GS	Hydrothermal + annealing at 150 °C, 2 h	Partial crystalline	52.7 wt%	Three-electrode	551 F/g at current density of 1.0 A/g	14
RuO_2/RGO	Hydrothermal	Partial crystalline	75 wt%	Three-electrode	497 F/g at current density of 0.5 A/g	15
a-RGO-RuO_2	Sol-gel + alkaline reduction of GO + annealing at 150 °C, 2 h	Amorphous	72.6 wt%	Two-electrode	509 F/g at current density of 1.0 A/g	This work

values are comparable to the best specific capacitances RGO-RuO_2 ever reported, as shown in Table 1. Note that most of the reported, higher value, specific capacitances originate from measurements on three electrode test cell configurations, which do not accurately predict the more realistic capacitances measured from two electrode test cell configurations that mimic the physical configuration of a commercially packaged supercapacitor.[23] In comparison to the a-RGO-RuO_2 in H_2SO_4, the specific capacitances of a-RGO-RuO_2 in Na_2SO_4 were much smaller, only 206.8 and 136.6 F/g at current densities of 1.0 and 20.0 A/g, respectively. The lower specific capacitance of a-RGO-RuO_2 in Na_2SO_4 is due to the shortage of protons within neutral Na_2SO_4, which are needed for the redox reaction of RuO_2.[6] The reduced capacitance of a-RGO-RuO_2 in Na_2SO_4 primarily originated from the electrical double layer formed from the adsorption of ions at the surface of a-RGO-RuO_2.

Rate performance, one of the most important characteristics of a supercapacitor, was exceptional for the a-RGO-RuO_2 system, particularly in H_2SO_4 (Fig. 8(a)). The respective capacitance retentions were 86.2% (H_2SO_4) and 66.1 % (Na_2SO_4) when the current density increased from 1.0 to 20.0 A/g. The uniform decorating of ultra-small RuO_2 nanoparticles across the RGO sheets, insures fast charge carrier transport between the current collector and the surface of the RuO_2. Moreover, a-RGO-RuO_2's nanopores and nanochannels acted as electrolyte reservoirs, assuring a short diffusion length of ions within the electrode.

Electrochemical impedance spectroscopy was performed to extend our understanding of a-RGO-RuO_2's electrochemical behavior. The Nyquist plots in Fig. 8(b) exhibited a typical arc in the high-frequency region and a straight line in the low-frequency region. The vertical shape of the straight lines in the low-frequency region indicated that a-RGO-RuO_2 in both electrolytes closely resemble an ideal capacitor, consistent with the results from the CV and GDC. The arc and the Warburg-type line (the slope of 45° portion of the curve) of the a-RGO-RuO_2 in H_2SO_4 was much shorter and smaller than those in Na_2SO_4, suggesting a lower charge transfer resistance and a more efficient electrolyte diffusion in H_2SO_4 than in Na_2SO_4.[20] This result was reasonable because the diffusion of H^+ protons via a hopping mechanism was much faster than the diffusion of Na^+ cations. The equivalent series resistances (ESR), determined by extrapolating the vertical portion of the plot to the real axis, were only 0.62 and 1.55 Ω for a-RGO-RuO_2 in H_2SO_4 and Na_2SO_4, respectively. The smaller ESR of a-RGO-RuO_2 in H_2SO_4 explained its higher rate capacity.

The cycling stability, a critical factor for the practical implementation of supercapacitor electrodes, was evaluated

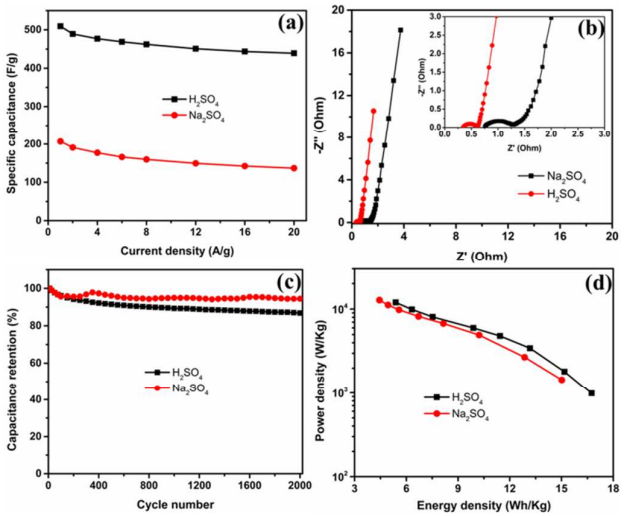

Figure 8. (a) Specific capacitance, (b) Nyquist plots, (c) cycling stability and (d) Ragone plots of RGO-RuO_2 in Na_2SO_4 and H_2SO_4 electrolytes, respectively.

using the galvanostatic charge/discharge technique at a current density of 2.0 A g^{-1}. As seen in Fig. 8c, the cycling stability of a-RGO-RuO_2 in Na_2SO_4 was slightly better than that in H_2SO_4. The capacitance of a-RGO-RuO_2 noticeably decreased ~5 % in the first 200 cycles for both electrolytes. Then, the capacitance of a-RGO-RuO_2 in H_2SO_4 electrolyte gradually decreased, whereas the capacitance in Na_2SO_4 was restored to 98 % its initial capacitance after 350 cycles before slightly decreasing again. The capacitance retentions of a-RGO-RuO_2 after 2000 charge/discharge cycles were 86.8 % for H_2SO_4 and 94.5 % for Na_2SO_4, indicating that a-RGO-RuO_2 has good long-term electrochemical stability.

The Ragone plots of a-RGO-RuO_2 are featured in Fig. 8d. Although the specific capacitance of a-RGO-RuO_2 in Na_2SO_4 was less than half of that in H_2SO_4, the energy density a-RGO-RuO_2 in Na_2SO_4 was comparable to that in H_2SO_4 due to extended working potential window, which was up to 1.5 V in the neutral electrolyte. The maximum energy densities of a-RGO-RuO_2 of 16.7 and 15.0 Wh/kg in H_2SO_4 and Na_2SO_4, respectively, were achieved at the current density of 1.0 A/g, corresponding to the power density of about 1000 W/Kg. More interestingly, at the high power density of 10 kW/kg, a-RGO-RuO_2 delivered a reasonable energy density of 6.3 Wh/Kg, indicating that a-RGO-RuO_2 is a promising electrode material for high power applications.

Conclusions

We report a facile approach to prepare a-RGO-RuO_2 for supercapacitor applications by an *in- situ* sol-gel deposition of RuO_2 nanoparticles on the surface of GO, followed by the reduction of GO in a strong alkaline medium at low temperature. The combination of the sol-gel route and the reduction of graphene oxide at low temperature resulted in ultrafine, hydrated amorphous RuO_2 nanoparticles with the size of only 1.0 – 2.0 nm, which uniformly decorated the surfaces of the RGO sheets. The excellent specific capacitance (509 F/g) obtained in H_2SO_4 electrolyte was the best value ever reported for RGO-RuO_2, measured from a two-electrode test cell configuration.

The a-RGO-RuO_2 exhibited a superior rate performance with capacitance retention of 86 % by increasing the current density from 1.0 to 20.0 A/g. The a-RGO-RuO_2 also showed good electrochemical cycling stability of 86.8 % capacitance retention after 2000 cycles. The excellent capacitive properties of a-RGO-RuO_2 were attributed to the uniform anchoring of ultra-small, hydrated amorphous RuO_2 nanoparticles on the surface of RGO sheets, resulting in synergistic effects between them. RGO sheets serve as conductive path for RuO_2 nanoparticles while RuO_2 nanoparticles decorating the surface of RGO sheets act as spacers to prevent the restacking of RGO sheets, creating nanopores and nanochannels and maximizing the surface area of a-RGO-RuO_2. Considering the facile synthesis approach and the excellent capacitive properties, a-RGO-RuO_2 has emerged as a promising electrode material for practical high-performance supercapacitor applications.

Acknowledgements

This work was supported in part by the U.S. Department of Energy, Office of Science, Office of Workforce Development for Teachers and Scientists (WDTS) under the Visiting Faculty Program (VFP). The research used resources of the Center for Functional Nanomaterials, which is a U.S. DOE Office of Science Facility, at Brookhaven National Laboratory under Contract No. DE-SC0012704.

References

1 L. L. Zhang, R. Zhou, and X. S. Zhao, *J. Mater. Chem.*, 2010, **20**, 5983.
2 Y. Huang, J. Liang, and Y. Chen, *Small*, 2012, **8**, 1805.
3 H. J. Choi, S. M. Jung, J. M. Seo, D. W. Chang, L. Dai, and J.-B. Baek, *Nano Energy*, 2012, **1**, 534.
4 P. Simon and Y. Gogotsy, Materials for electrochemical capacitors, *Nat. Mater.*, 2008, **7**, 845.
5 B. Conway, V. Birss, J. Wojtowicj, *J. Power sources*, 1997, **66**, 1.
6 G. Wang, L. Zhang, J. Zhang, *Chem. Soc. Rev.*, 2012, **41**, 797.
7 Z. S. Wu, D.-W. Wang, W. Ren, J. Zhao, G. Zhou, F. Li, and H.-M. Cheng, *Adv. Funct. Mater.*, 2010, **20**, 3595.
8 A. K. Mishra and S. Ramaprabhu, *J. Phys. Chem. C,* 2011, **115**, 14006.
9 J. Zhang, J. Jiang, H. Li and X. S. Zhao, *Energy Environ. Sci.*, 2011, **4**, 4009.
10 R. B. Rakhi, W. Chen, D. Cha and H. N. Alshareef, *J. Mater. Chem.*, 2011, **21**, 16197.
11 Y. Chen, X. Zhang, D. Zhang and Y. Ma, J. Alloy. Compd., 2012, **511**, 251.
12 Y. Chen, X. Zhang, D. Zhang and Y. Ma, *J. Alloy. Compd.*, 2012, **541**, 415.
13 N. Soin, S. S. Roy, S. K. Mitra, T. Thundat and J. A. McLaughlin, *J. Mater. Chem.*, 2012, **22**, 14944.
14 N. Lin, J. Tian, Z. Shan, K. Chen, W. Liao, *Electrochimica Acta,* 2013, **99**, 219.
15 J. Y. Kim, K.-H. Kim, S.-B. Yoon, H.-K. Kim, S.-H. Park and K.-B. Kim, *Nanoscale*, 2013, **5**, 6804.
16 J. Shen, T. Li, W. Huang, Y. Long, N. Li, M. Ye, *Electrochimica Acta*, 2013, **95**, 155.
17 W. Wang, S. Guo, I. Lee, K. Ahmed, J. Zhong, Z. Favors, F. Zaera, M. Ozkan and C. S. Ozkan, Sci. Rep., 2013, **4**, 4452.
18 L. Deng, J. Wang, G. Zhu, L. Kang, Z. Hao, Z. Lei, Z. Yang, Z.-H. Liu, *J. Power Source*, 2014, **248**, 407.
19 C. Zhang, H. Zhou, X. Yu, D. Shan, T. Ye, Z. Huang and Y. Kuang, *RSC Adv.*, 2014, **4**, 11197.
20 V. H. Pham, T. Gebre and J. H. Dickerson, *Nanoscale*, 2015, **7**, 5947.
21 X. Fan, W. Peng, Y. Li, X. Li, S. Wang, G. Zhang and F. Zhang, *Adv. Mater.*, 2008, **20**, 4490.
22 L. L. Zhang, X. Zhao, M. D. Stoller, Y. Zhu, H. Ji, S. Murali, Y. Wu, S. Perales, B. Clevenger and R. S. Ruoff, *Nano Lett.*, 2012, **12**, 1806.
23 M. D. Stoller and R. S. Ruoff, *Energy Environ. Sci.*, 2010, **3**, 1294.
24 S. Park, K.-S. Lee, G. Bozoklu. W. Cai, S. B. T. Nguyen, and R. S. Ruoff, *ACS Nano*, 2008, **2**, 572.
25 J. P. Zheng, P. J. Cygan and T. R. Jow, *J. Electrochem. Soc.*, 1995, **142**, 2699.
26 H. Kim and B. N. Popov, *J. Power Sources*, 2012, **104**, 52.
27 S. Park, J. An, I. Jung, R. D. Piner, S. J. An, X. Li, A. Velamakanni, and R. S. Ruoff, *Nano Lett.*, 2012, **9**, 1593.
28 K. Naoi, S. Ishimoto, N. Ogihara, Y. Nakagawa and S. Hatta, *J. Electrochem. Soc.*, 2009, **156**, A52.

29 H. Xia, Y. S. Meng, G. Yuan, C. Cui and L. Lu, *Electrochem. Solid-State Lett.*, 2012, **15**, A60.